RSC Advances

PAPER

View Article Online
View Journal | View Issue

Cite this: *RSC Adv.*, 2024, **14**, 24398

Haloarchaeal poly[(3-hydroxybutyrate)-*co*-(3-hydroxyvalerate)] composite films reinforced with graphene nanoplatelets as a biomaterial for skin tissue engineering†

Prajakta Praveen Bhende,[a] Joephil D. Dias,[a] Honey Srivastava,[b] Rashmi Chauhan,[b] Sachin Waigaonkar,[c] Anasuya Ganguly[a] and Judith M. Braganç[a]*[a]

Received 28th January 2024
Accepted 6th July 2024

DOI: 10.1039/d4ra00713a

rsc.li/rsc-advances

Halophilic archaea are an untapped source for a wide range of applications. This study explores the potential of a copolymer poly[(3-hydroxybutyrate)-*co*-(3-hydroxyvalerate) (PHBV), naturally synthesized by the halophilic archaeon, *Halogeometricum borinquense* E3, as a potential candidate for a tissue engineering biomaterial. Composites and blends from natural PHBV were fabricated with poly(L-lactic acid) (PLLA), poly(ε-caprolactone) (PCL) and graphene nanoplatelets (GNP) to enhance the properties of the material. This significantly improved the tensile strength of the blend to 4.729 MPa (359%). The reinforcement with 0.3% w/v of GNP further increased the tensile strength to 13.268 MPa (981%). Characterization of the films was done using ATR-FTIR, XRD, TGA, and SEM. The haloarchaeal PHBV exhibited the highest porosity ergo the highest swelling percentage while the PHBV/GNP showed the least. All the films showed good biocompatibility compared to tissue culture plastic (TCP). The viability of HaCaT cells and L929 fibroblast cells was maximum on the PHBV/PLLA/PCL blend albeit no significant change in the cell viability was observed in the graphene-reinforced nanocomposite. The films were also highly hemocompatible (<5% hemolysis).

1 Introduction

The field of regenerative medicine and tissue engineering depends on the selection of an appropriate biomaterial to be used as a scaffold, cells of the tissue to be engineered and the factors required for growth and differentiation of the cells. Natural-origin polymers are often preferred to be used as a biomaterial.[1,2] Any polymer to be used as a biomaterial should be non-toxic, biocompatible, and biodegradable. It should be porous and have a wide surface area to promote cell–cell interaction and facilitate the transport of nutrients and waste products. It should possess suitable mechanical strength to withhold the developing tissue and thus promote cell adhesion, growth, and differentiation.[3,4]

Polyhydroxyalkanoates (PHAs) are a group of naturally occurring polyesters synthesized by microorganisms due to an imbalance in essential nutrients with excessive carbon and stored as insoluble cytoplasmic inclusions or "carbonosomes". These granules can be enzymatically depolymerized and used as a source of carbon.[5,6] PHAs are versatile and their properties change according to the number of carbon atoms present in the polymer chain. PHAs with 3–5 carbon atoms are classified as short chain length polymers (scl); 6–14 carbon atoms are classified under medium chain length (mcl) and more than 14 carbon atoms are grouped as long chain length (lcl). Based on the available carbon source, the microorganisms can synthesize either a homopolymer containing the same repeating unit *e.g.*, poly(3-hydroxybutyrate) or copolymers *e.g.*, poly[(3-hydroxybutyrate)-*co*-(3-hydroxyvalerate)].[7,8]

In this study, we explored the application of intrinsically produced copolymer, poly[(3-hydroxybutyrate)-*co*-(3-hydroxyvalerate)] by haloarchaeon, *Halogeometricum borinquense* E3, as a potential biomaterial for skin tissue engineering. Haloarchaea belong to the family Halobacteriaceae, within the third Domain of Life, Archaea. These are extremely halophilic organisms requiring about 100–300 g L^{-1} of NaCl for their growth.[9,10] Haloarchaea are advantageous to be used for PHA production as they are non-pathogenic and do not contain lipopolysaccharide (LPS) as in Gram negative bacteria. LPS endotoxin gets co-extracted with the polymer thereby causing immunogenic and pyrogenic reactions.[11]

[a]*Department of Biological Sciences, Birla Institute of Technology and Science, Pilani KK Birla Goa Campus, Goa, India. E-mail: judith@goa.bits-pilani.ac.in*

[b]*Department of Chemistry, Birla Institute of Technology and Science, Pilani KK Birla Goa Campus, Goa, India*

[c]*Department of Mechanical Engineering, Birla Institute of Technology and Science, Pilani KK Birla Goa Campus, Goa, India*

† Electronic supplementary information (ESI) available. See DOI: https://doi.org/10.1039/d4ra00713a

PHAs are an intriguing option for biomaterial owing to their lack of toxicity towards cells and blood, capacity for biodegradation, and non-carcinogenicity. A lot of research is being done investigating the applications of PHA in hard tissue engineering (bone,[12] cartilage,[13] and tendon), wound healing,[14] nerve tissue,[15] vascular tissue repair[16,17] and as bio-absorbable sutures.[18] Due to its lower degree of crystallinity, PHBV is preferred over PHB for medical applications. The degradation of heteropolymers is also higher than homopolymers in the human body.[19] PHBV as calcium silicate composites have been studied for cartilage tissue engineering[20] while blends of PHBV with PCL, pullulan, chitosan or hydroxyapatite based scaffolds have been explored for bone tissue engineering applications.[21–23] Besides some studies have explored the use of PHBV composites with fibronectin or collagen in wound healing and vascular tissue engineering.[24,25]

Despite its remarkable properties, PHAs (especially scl's) have drawbacks like high fragility, low impact resistance, reduced elongation at break, and poor mechanical strength. In this study, we have blended PHBV with 1 wt% poly(L-lactic acid) (PLLA) and 1 wt% poly(ε-caprolactone) (PCL). PLLA is a homopolymer obtained from natural resources like sugarcane and corn starch using sustainable catalysts like sorbitol. It provides improved mechanical properties to the blend for effective support in prolonged regenerative processes. PLLA is also non-toxic, it degrades to form lactic acid which is a natural metabolite and is excreted as carbon dioxide and water.[22,23] Jamal *et al.* 2024 (ref. 24) used PHBV and PLLA to develop a bilayer composite membrane for growth and proliferation of MC3T3 pre-osteoblastic cells. PCL is an aliphatic polyester synthesized by the ring-opening polymerization of ε-caprolactone. Its porous nature provides an increased surface area for cell–cell interaction. It is also known to enhance the growth and differentiation of fibroblasts.[25]

Graphene has a sp^2 hybridized carbon in a 2D honeycomb lattice structure. This along with electronic distribution gives rise to a large surface area, unique electrical conductivity, and excellent mechanical properties. The availability of a large surface area facilitates the adsorption of proteins and growth factors thereby promoting cell adhesion and growth.[26,27] It is critical to assess the cytotoxicity and biocompatibility of any material before its use in biomedical applications. The cytotoxicity of graphene is directly related to its concentration used, the length of incubation and the structure and type of graphene used.[28] Salesa *et al.* 2022 (ref. 29) reported that graphene nanoplatelets (GNPs) at non-cytotoxic levels showed significant proliferative activity of HaCaT cells. Moreover GNPs were capable of upregulating almost half of the thirteen genes which were required for wound healing and skin tissue engineering.

The use of graphene for various biomedical applications is gaining momentum. Suvarnaphaet *et al.* 2019 (ref. 30) developed a biodegradable electrode patch made of graphene and PHA which could detect an electrocardiogram signal triggered by electrical activity through the heart. Moschetta *et al.* 2021 (ref. 31) made a biocompatible neuronal interface using P(3HB) and GNP which showed potential for interfacing with primary neurons in order to target disorders of the central nervous system.

This study is the first report to analyse archaeal derived PHBV/PLLA/PCL-graphene nanoplatelets composite for the proliferation of keratinocytes and fibroblasts with potential for skin tissue engineering. Haloarcheal PHBV (1% w/v), PLLA (1% w/v), PCL (1% w/v), and GNP (0.3% w/v) were used to prepare a blend/nanocomposite using the solvent casting method. The synthesised blends and graphene nanocomposites were further characterised to assess their ultrastructure, chemical composition, functional group analysis, thermal and mechanical properties. Concomitantly, their biological characterisation was aimed to analyse the hemocompatibility, biocompatibility and proliferative capacity of human skin keratinocytes HaCaT cells and mouse fibroblast L929 cells for potential applications in skin tissue engineering.

2 Materials

The polymer, PCL of practical grade having molecular weight 9000–11 000 g mol^{-1} with melt flow index of 22–24 g/10 min was purchased from Otto Chemie Pvt. Ltd. Mumbai, India, and medical grade PLLA of molecular weight 100–140 kDa was purchased from Nomisma Healthcare Pvt. Ltd. Gujarat, India. The graphene nanoplatelets of particle size 5 μm were purchased from Sigma-Aldrich. Stains used for confocal microscopy were Fluoroshield with DAPI from Sigma-Aldrich; and Acti-stain™ 555 Fluorescent Phalloidin from Cytoskeleton, Inc. Analytical grades of chloroform and diethyl ether from Thomas Baker were used. Sodium cacodylate and osmium tetroxide were purchased from Sigma-Aldrich. The haloarchaeal strain *Halogeometricum borinquense* E3 (AB904833) was isolated previously in our laboratory.[32] All cell culture materials, media components and sodium hypochlorite were purchased from Himedia, India unless mentioned otherwise. The HaCaT cell line was a kind gift from NBIL, Bengaluru, India while the L929 fibroblasts were purchased from NCCS Pune, India.

3 Methods

3.1 Production of PHBV polymer and preparation of blends

3.1.1 Growth of *Halogeometricum borinquense* E3. *Halogeometricum borinquense* E3 was maintained on Extremely Halophilic agar Medium (EHM). A loopful of culture was inoculated in 100 mL of EHM broth (per litre: NaCl 250 g; $MgSO_4 \cdot 7H_2O$ 20 g; KCl 2 g; yeast extract 10 g; $CaCl_2 \cdot 2H_2O$ 0.36 g; NaBr 0.23 g; $NaHCO_3$ 0.06 g; peptone 5 g; $FeCl_3$ trace amounts; pH 7–7.4) and incubated at 37 °C, 120 rpm, for 4 days in an incubator shaker (Scigenics Biotech ORBITEK). 5% of the culture inoculum was then transferred into 1 L of NaCl-Glucose Synthetic Medium (NGSM) for polymer production: [per litre: NaCl 200 g; $MgCl_2 \cdot 6H_2O$ 13 g; KCl 4 g; $CaCl_2 \cdot 2H_2O$ 1 g; $NaHCO_3$ 0.2 g; $FeCl_3$ 0.005 g; KH_2PO_4 0.5 g; dextrose 2%; pH 7–7.4). The culture was incubated for 8–10 days at 37 °C, 120 rpm.

3.1.2 Polymer recovery and film synthesis. *Halogeometricum borinquense* E3 grown in NGSM with 2% glucose was centrifuged at 10 000 rpm for 15 min at 4 °C (Thermo Scientific

Heraeus Multifuge X3 FR Centrifuge) to obtain the biomass. 4% NaOCl was added to the biomass and incubated on a rocker for 2–3 h. The mixture was centrifuged again using the same conditions. The supernatant was discarded, and the pellet was washed with distilled water and diethyl ether followed by reflux with hot chloroform. The chloroform-polymer mixture was poured into a clean glass Petri dish and kept in the cold room for the evaporation of the solvent to obtain the polymer film.

3.2 Preparation of PHBV derived blend and composite

Halogeometricum borinquense E3 derived PHBV, was blended by using 1% (w/v) of the polymer with 1% (w/v) PLLA, 1% (w/v) PCL, and 0.3% (w/v) GNP. The polymers were dissolved in chloroform at 60 °C till homogenous using a vortex mixer. The mixture was poured into a clean dry glass Petri dish. The composite containing the GNPs was sonicated for 5 minutes before pouring to obtain a uniform dispersion of the GNPs in the solution. The dispersions were left undisturbed for 24 hours in the cold room for the solvent to evaporate and form a film. The average thickness of each film was measured using a micrometer screw gauge.

3.3 Physicochemical characterization

3.3.1 Field emission scanning electron microscopy (FESEM). The surface morphology of the polymer film was examined by scanning electron microscope (Quanta FEG 250). The samples were coated with a 4 nm coating of Au–Pd (LEICA EM ACE 200 sputter coater) before imaging.

3.3.2 X-ray diffraction (XRD). The X-ray diffraction of the films was performed using Bruker D-8 Advance X-ray diffractometer. The samples were analyzed from 10–30° with a scanning speed of 5° min^{-1}.

3.3.3 Fourier transform infrared spectroscopy (FTIR). The FT-IR spectra of the haloarchaeal polymer and the films were obtained using Spectrum 2 ATR-FTIR, PerkinElmer. The scans were recorded from 400 cm^{-1} to 4000 cm^{-1}.

3.3.4 Mechanical properties. The ultimate tensile strength (UTS), Young's modulus, and elongation at break were assessed using a Dynamic Mechanical Analyzer (DMA Q 800) supplied by TA Instruments, USA. The polymer films with a dimension of 35 mm × 12 mm were mounted using tension film clamps to calculate the stress *vs.* strain behavior. 1.0 N min^{-1} was the rate of ramp force. Calibration of the device and clamps was carried out before use.

3.3.5 DSC-TGA. The DSC-TGA analysis of the films were performed on SDT 600 TA Instruments Trios V5.2.2.47561 at a heating rate of 10 °C min^{-1} from room temperature up to 800 °C under nitrogen. For DSC, the samples were first heated up to 150 °C at a rate of 10 °C min^{-1}, cooled and then reheated to 300 °C under a flowing nitrogen atmosphere.

3.3.6 Swelling percentage and porosity. Pre-weighed films of PHBV, its blend and composite were soaked in phosphate-buffered saline (PBS). The films were taken out after 1 hour and 24 hours and excess PBS was removed. The films were weighed again (Sartorius Secura Milligram Balance). The swelling percentage was calculated using the formula:

$$\%\ \text{swelling} = \frac{(W_s - W_d)}{W_d} \times 100 \quad \text{(A1)}$$

where W_s = weight of swollen films, W_d = weight of dry films.

To calculate the porosity of the films, the films of known weight were immersed in absolute ethanol for 1 h and incubated at 30 °C. After incubation, the films were taken out and the excess ethanol was removed using a blotting paper. The films were weighed again. Porosity was calculated in terms of percentage using the formula below:[33]

$$\%\ \text{porosity} = \frac{(W_w - W_d)}{\rho v} \times 100 \quad \text{(A2)}$$

where W_d = dry weight of the films, W_w = wet weight of the films, ρ = density of ethanol at 30 °C, v = volume of swollen scaffolds.

3.4 Biological characterisation

3.4.1 Assessment of *in vitro* biocompatibility. The biocompatibility of the *Halogeometricum borinquense* E3 derived PHBV polymer, its blend and composite were evaluated on human keratinocyte cell line (HaCaT) and mouse fibroblast cell line (L929).

The cell lines were maintained in Dulbecco's Minimal Essential Medium (DMEM) supplemented with 10% Fetal Bovine Serum (FBS) and 0.1% antibiotic–antimycotic solution. The polymer films were sterilized by immersing in 70% ethanol and UV irradiated for 1 h on each side. Two washings with sterile PBS were given and the films were placed inside a tissue culture grade 48-well plate. A 70% confluent flask of each cell line was trypsinized. The cells were counted using a cell counter (Bio-Rad TC-20). 1×10^4 cells were seeded on the sterile films. The plate was incubated in a humidified environment of 5% CO_2 at 37 °C. Media change was given every alternate day. The cell viability was evaluated spectrophotometrically by (3-[4,5-dimethylthiazol-2-yl]-2,5 diphenyl tetrazolium bromide) (MTT) assay after day 1, day 2, day 5, and day 7. A concentration of 5 mg per ml MTT was added to the wells and incubated for 4 h. The purple formazan crystals were solubilized using dimethyl sulfoxide (DMSO). The plate was shaken for 5 min and the contents were transferred to a 96-well microtiter dish. The absorbance was read at 575 nm. Cells grown in a tissue culture grade 48 well were considered as control.[34,35]

3.4.2 Microscopy. The HaCaT and L929 cells were cultured on the films for 2 days. After incubation, the medium was removed, and the films were washed gently with sterile PBS. For fixation, 2.5% glutaraldehyde in 0.1 M sodium cacodylate was added to the films and kept at 4 °C overnight. The films were washed 2–3 times with PBS and post-fixed in 1% osmium tetroxide in the dark. This was followed by dehydration with an increasing series of ethanol–20%, 30%, 50%, 70%, 90%, and 100%. The samples were later sputter-coated with a 4 nm coating of Au–Pd and visualized under a scanning electron microscope.[12,36]

For confocal microscopy, the films containing the cells were fixed in 4% paraformaldehyde (pH 7.0) in PBS. The samples were washed 2–3 times with PBS. The cells were permeabilized with 0.1% Triton-X-100 followed by another round of washing. The samples were stained with Acti-stain 555 Fluorescent

Phalloidin in the dark for 30 min at room temperature. 2–3 washes of PBS were given, and the samples were counterstained with DAPI and observed under a confocal microscope (Olympus Corporation FV3000).[37,38]

3.4.3 Adsorption of proteins on the surface of the films. The films were incubated in PBS containing 1% v/v FBS for 1 h at 37 °C. After incubation, the films were then immersed in 2.0 wt% sodium dodecyl sulfate (SDS) in PBS for 20 hours. The proteins adsorbed on the surface of the films were estimated by bicinchoninic acid assay (BCA) and expressed as the mean of adsorbed proteins in μg per mm^3 of the film. Bovine serum albumin (BSA) was used to plot the standard calibration curve.[39]

3.4.4 Degradation of the films *in vitro*. The study of *in vitro* degradation of the films was performed using the protocol described by Aghmiuni *et al.* 2020 (ref. 33) with slight modification. Pre-weighed films were immersed into PBS containing lysozyme and incubated at 37 °C for 7, 14, 21 and 28 days. At the end of the incubation period, the films were carefully taken out and rinsed with deionised water. The films were dried in the oven at 40 °C and weighed again till a constant weight was obtained. The percentage degradation was calculated using the formula given below:

$$\%\ \text{degradation} = \frac{(W_i - W_f)}{W_i} \times 100 \quad \text{(A3)}$$

where W_i = initial weight of the films, W_f = final weight of the films.

The ultrastructure of the degraded films was observed by SEM (ESI data S3†).

3.4.5 Evaluation of hemocompatibility of the films. 5 mL blood was withdrawn using standard ethical procedures from the participating volunteer at the Institute medical center with the help of the medical staff. An 8 : 10 dilution of the blood was made with sterile normal saline (0.85% NaCl). The films were incubated in normal saline for 30 min at 37 °C. The saline was carefully decanted out and diluted blood was added to the films. The films were incubated at 37 °C for 60 min. After the incubation, the mixture was centrifuged at 2000 rpm for 10 min. The absorbance of the supernatant was read at 545 nm. Blood incubated with sodium carbonate and normal saline was considered a positive and negative control respectively. The degree of hemolysis was evaluated as follows:

$$\%\ \text{hemolysis} = \frac{\text{Abs}_S - \text{Abs}_{NC}}{\text{Abs}_{PC} - \text{Abs}_{NC}} \times 100 \quad \text{(A4)}$$

where Abs_S is the absorbance of sample, Abs_{PC} is the absorbance of positive control and Abs_{NC} is the absorbance of negative control.[40]

4 Statistics

All experiments were conducted in triplicates. The quantitative data is expressed as mean ± standard error of mean. Statistical analysis was done using Two-way ANOVA with Tukey's multiple comparisons test in GraphPad Prism 6 (GraphPad Software Inc) and Origin Pro 2023b (Origin Lab Corporation). Values of $p < 0.05$ were considered significant.

5 Results and discussions

5.1 Production of PHBV polymer and preparation of blends and composites

5.1.1 Growth of *Halogeometricum borinquense* E3. *Halogeometricum borinquense* E3 was grown in EHM broth for 4 days (OD_{600} = 1.8) and 5% of this was used as inoculum for 1 L of NGSM medium for polymer production. 20 mL of the sample was withdrawn from NGSM during each time point for the determination of absorbance (A_{600nm}), Cell Dry Weight (CDW), and polymer production. The maximum accumulation of the polymer was observed on day 4 *i.e.*, 78.51% of CDW. A consistent drop in the pH was observed and on the day of harvest, the pH was recorded to be 5.6. This is attributed to the formation of acidic metabolites. A gradual decline in the polymer accumulation was noticed after day 4 and on the day of harvest, it was recorded to be 69.01% of CDW. A graphical representation of the growth profile is given in Fig. 1. The use of halophilic archaea to produce polyhydroxyalkanoates (PHA) is extremely advantageous. Halophilic archaea thrive when the salinity is greater than 15%. This itself retards the growth of other contaminating organisms. The intracellular polymer can be recovered from the culture by lysing the microbial cells in distilled water, thereby reducing the downstream costs. Besides they can utilize cheap carbon substrates for synthesizing PHA.

5.1.2 Polymer recovery and film synthesis. The PHBV polymer obtained after the hypochlorite treatment of the cell pellet was dissolved in chloroform at 60 °C. The solvent from the mixture evaporated leaving behind a pale orange film with a rough upper surface and a smooth bottom surface (Fig. 2). *Hgm. borinquense* E3 produces an intracellular carotenoid pigment, bacterioruberin.[41] However, treatment with NaOCl led to bleaching of the pigment, producing a cream-colored film (Fig. 2a). The average thickness of the film was observed to be 77 μm. *Hgm. borinquense* E3 innately produced a copolymer poly [(3-hydroxybutyrate)-*co*-(3-hydroxyvalerate)] (PHBV) with 30 mol% 3-HV units (ESI data S1†). Limited studies are available on the synthesis of PHBV by *Halogeometricum* spp. A report by Mahansaria *et al.* (2020) evaluated the production of PHBV from *Halogeometricum borinquense* RM-G1 using various carbon

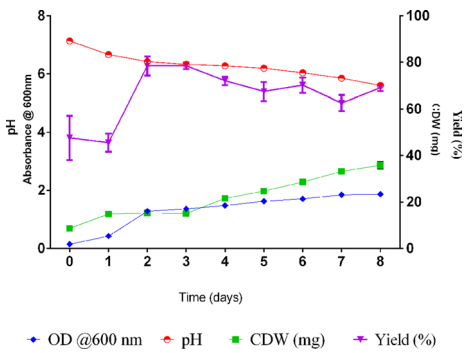

Fig. 1 The growth profile of *Halogeometricum borinquense* E3 was studied for 8 days in NaCl-Glucose Synthetic Medium (NGSM) with 2% glucose as the carbon source. Cell Dry Weight (CDW), PHBV production, and the pH of the medium was measured every 24 h.

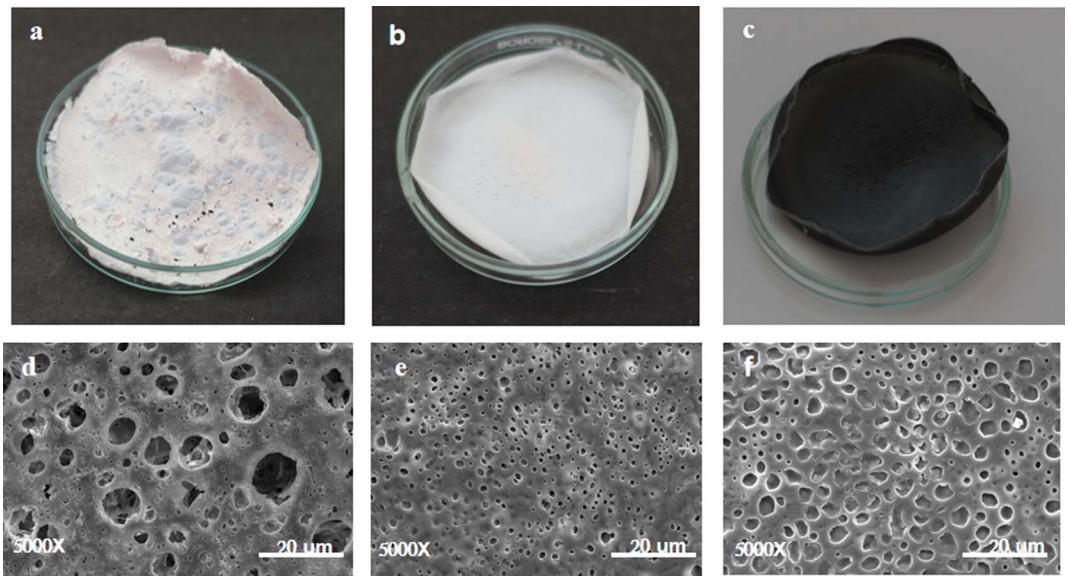

Fig. 2 (a) PHBV polymer film derived from haloarchaea *Halogeometricum borinquense* E3 (b) PHBV/PLLA/PCL blend of 1% w/v haloarchaeal PHBV, 1% w/v PLLA and 1% w/v PCL (c) PHBV/PLLA/PCL/GNP composite of 1% w/v haloarchaeal PHBV, 1% w/v of PLLA, 1% w/v of PCL, and 0.3% w/v of GNP. Scanning electron microscopic images of (d) *Halogeometricum borinquense* E3 derived PHBV, (e) PHBV/PLLA/PCL and (f) PHBV/PLLA/PCL/GNP composite. The pore size of haloarchaeal PHBV and its composites was calculated and reported as mean ± SEM. Statistical analysis was done using the Student's *t*-test.

sources with a maximum PHBV accumulation of 66.80% ± 1.69 of cell dry mass within 72 hours of production when 1.6% glycerol was used as a carbon source.[42] The 3-HV content reported was 10.21 mol%. Previous studies on *Hgm. borinquense* E3 conducted in our laboratory reported the maximum PHBV accumulation of 50.4 ± 0.1 and 45.7 ± 0.19% on the 7th day when the carbon source was sugarcane bagasse hydrolysate of 25% and 50% respectively.[43] When 2% glucose was used as a carbon source, the accumulated PHBV was 73.51% ± 1.7%.[32] The results of this study also showed a consistent accumulation of 78.51% PHBV.

5.1.3 Preparation of PHBV derived blends. Haloarchaeal PHBV was blended with PLLA and PCL polymers to give PHBV/PLLA/PCL blends (Fig. 2b) and with graphene nanoplatelets to give PHBV/PLLA/PCL/GNP nanocomposite films (Fig. 2c) (Table 1). The average thickness of each film was measured using a micrometer screw gauge and was observed to be 110 μm and 120 μm respectively as compared to the native haloarchaeal polymer which was 77 μm. There was no phase separation observed. Inorder to create a robust architectural structure and functionality that is necessary for skin tissue engineering, the composite needs to meet certain conditions. Mechanical attributes like Young's modulus, ultimate tensile strength and elongation at break are crucial specifications that endow the scaffold with its structural property and longevity.[44] PHBV as a biopolymer has poor mechanical strength and hence can be supplemented with fillers like PLLA and PCL to improve its mechanical properties. PCL and PHBV when blended in concentrations of 5–10% with PLLA improved the Young's modulus by up to 25%, the tensile strength increased by almost 50% and the elongation at break by 4000%.[45]

5.2 Physicochemical characterisation

5.2.1 FESEM. The surface morphology of the *Halogeometricum borinquense* E3 derived PHBV was observed to be rough and undulating with a random arrangement of pores on the surface (Fig. 2d). The average pore size was observed to be 3.58 ± 0.18 μm (95% confidence interval). A slight reduction in the range of pore size was noticed in the PHBV/PLLA/PCL blend. The average pore size was found to be 2.05 ± 0.28 μm (Fig. 2e). The PHBV/PLLA/PCL/GNP composite film appeared dense. The pores in this case appeared like "hollow depressions" in which

Table 1 *Halogeometricum borinquense* E3 derived PHBV and preparation of its blend and/or nanocomposite films

Sr. no	Blend	Composition	Average thickness (μm)
1	Native polymer	*Halogeometricum borinquense* E3 derived polymer	77
2	PHBV/PLLA/PCL	1% w/v *Halogeometricum borinquense* E3 derived polymer + 1% w/v poly-L-Lactic acid + 1% w/v poly-ε-caprolactone (PCL)	110
3	PHBV/PLLA/PCL/GNP	1% w/v *Halogeometricum borinquense* E3 derived polymer + 1% w/v poly-L-Lactic acid + 1% w/v poly-ε-caprolactone (PCL) + 0.3% w/v graphene nanoplatelets (GNP)	120

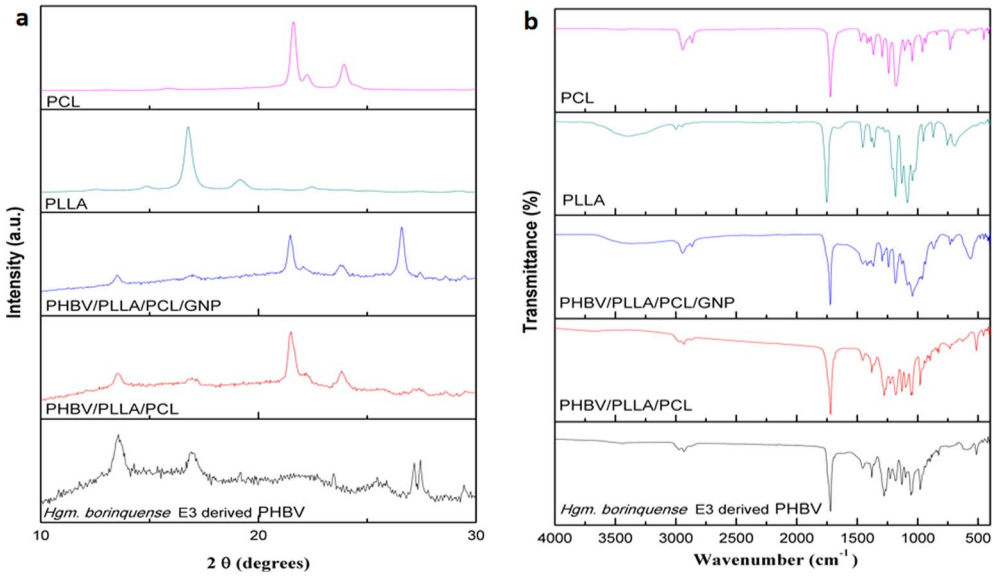

Fig. 3 (a) X-ray diffractogram of *Halogeometricum borinquense* E3 derived PHBV and its blend/composite. (b) FT-IR spectra of *Halogeometricum borinquense* E3 derived PHBV and its blend and composite.

the GNPs were embedded (Fig. 2f). The average pore size was calculated to 2.08 ± 0.23 μm. Ideal skin tissue composites should posess a porous architecture to resemble the extracellular matrix of the skin thus promoting adhesion and proliferation of the cells. Composites also improve hydrophilicity and function as a channel for movement of metabolites and nutrients which eventually helps in tissue development.[46,47]

5.2.2 XRD. The XRD pattern of haloarchaeal PHBV, its blends/composite is given in Fig. 3a. The X-ray diffraction pattern of *Halogeometricum borinquense* E3 derived PHBV recorded prominent peaks at 2θ = 13.5°, 16.88°, 27.44° and 29.48°. These values correspond to the (020), (110), (121), and (002) reflections of the crystalline planes.[48] In PHBV/PLLA/PCL blend, the main peaks were obtained at 2θ = 13.5°,17.0°, 21.58°, 23.58° and 27.24°. The main characteristic peak of the haloarcheal PHBV at 13.5° was also expressed in the PHBV/PLLA/PCL blend and PHBV/PLLA/PCL/GNP composite. Broadening of the peaks in the blend suggest decrease in crystallinity and point towards semi-crystalline nature of the polymer. The peaks for PLLA and PCL are also exhibited in the blend. PCL showed diffraction peaks at 21.62°, 23.95° corresponding to (110) and (200) planes of orthorhombic crystalline phase.[49] The intense peak at 21.58° in the blend could be attributed to the PCL component. Pure PLLA exhibited a characteristic peak at 16.6° corresponding to (200) (100) planes which had a shift to 17.0° in the blend.[50] These shifts in the positions of the peaks

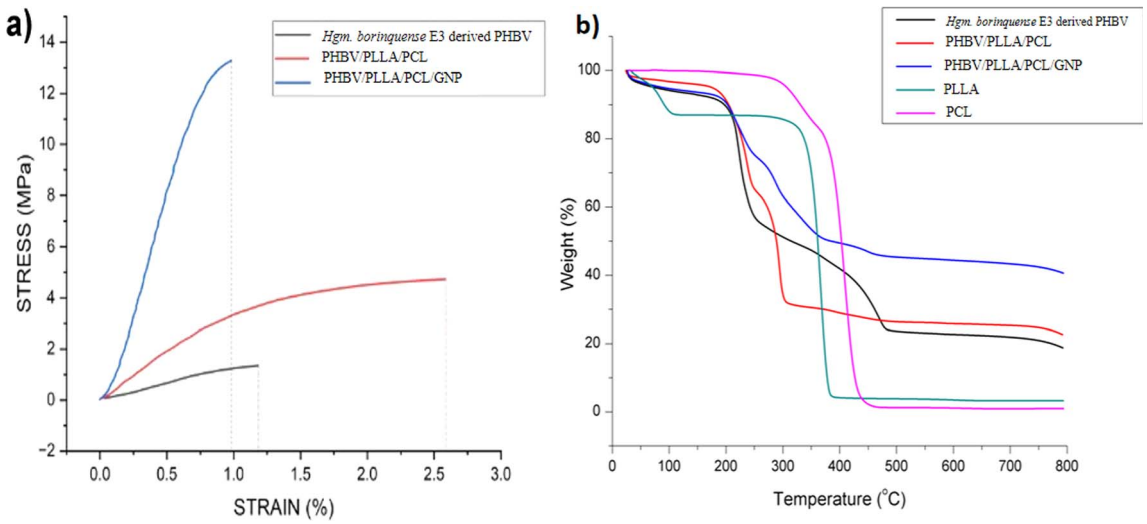

Fig. 4 (a) Stress *vs.* strain curve of PHBV derived from *Halogeometricum borinquense* E3 and its blend/composite. (b) Thermogravimetric curve of the haloarchaeal PHBV and its blend/composite[45] from 25 °C to 800 °C.

and the intensities are attributed to interactions between the individual polymers in the blend. In the PHBV/PLLA/PCL/GNP composite film, the intense crystalline peak of graphene was noticed at $2\theta = 26.5°$ signifying increased crystallinity.

5.2.3 FT-IR. The FT-IR spectrum of haloarchaeal PHBV, blend and nanocomposite is given in Fig. 3b. Characteristic peaks at 2995 cm^{-1} corresponds to C–H anti-symmetric stretch, 2952 cm^{-1} to C–H symmetric stretch and 1720 cm^{-1} correspond to C=O of ester bonds. The characteristic peak for symmetrical wagging of CH_3 group and C–O stretch were observed at 1386 cm^{-1} and in the region 1283 to 980 cm^{-1}, respectively.[51]

In the FT-IR spectra of PHBV/PLLA/PCL/GNP nanocomposite the intense peak of C=O of ester group at 1726 cm^{-1} shows the presence of PHBV. The medium intensity C–O stretching peaks are broadened due to interaction with GNP and are observed in the region 980–1350 cm^{-1}. Multiple small peaks were obtained in the region of 1500 cm^{-1} contributed by GNP. This is in agreement with the findings of Ahmed J. *et al.* (2021).[52] The changes in the peak intensity of the PHBV/PLLA/PCL/GNP could be related to the action of weak van der Waals forces.[53]

The FT-IR spectra of PLLA shows the characteristic broad peak corresponding to O–H stretch at 3400 cm^{-1}. The C=O of ester and C–O stretching peaks were observed in the region 1757 cm^{-1} and 1200–1069 cm^{-1}, respectively and the characteristic peak for symmetrical wagging of CH_3 group with medium intensity was observed at 1374 cm^{-1}. Similarly for PCL the C=O of ester and C–O stretching peaks were observed in the region 1725 cm^{-1} and 1246–1050 cm^{-1} respectively. In FT-IR spectra, the C–H stretching peaks were observed in the region 2975–2865 cm^{-1} with the characteristic asymmetric and symmetric stretch of C–H corresponding to CH_3 at 2931 cm^{-1} and 2865 cm^{-1} respectively. The C=O of PHBV, PLLA and PCL merged together and gave an intense peak at 1723 cm^{-1} showing the highly ordered crystalline structure. The peak for symmetrical wagging of CH_3 group with medium intensity was observed at 1374 cm^{-1} and the medium intensity C–O stretch were observed in the region 1282–982 cm^{-1}.

5.2.4 Mechanical properties. The stress *vs.* strain curve of haloarchaeal PHBV, its blend and composite is shown in Fig. 4a and the respective values are tabulated in Table 2. The ultimate tensile strength of the haloarchaeal PHBV was recorded as 1.42 ± 0.3 MPa with 1.03 ± 0.2% elongation at break. The Young's modulus was 148.25 ± 2.1 MPa. These results are in coherence with the study conducted by Kuppan *et al.* (2011) where the tensile strength of solvent-cast 2D PHBV film was reported as 1.57 MPa.[54] Blending the PHBV with PLLA and PCL significantly increased the ultimate tensile strength by 359% to 5.1 ± 0.5 MPa with a 4.11 ± 2.2% elongation at break and Young's modulus was 352.75 ± 30 MPa. Reinforcement with GNP further increased the ultimate tensile strength of native PHBV by 981% to 13.94 ± 1.2 MPa and Young's modulus was observed to be 396.25 ± 42 MPa. However, the elongation at break was seen to reduce to 0.88 ± 0.1%. The immense improvement in the tensile strength and the elastic modulus could be due to the strong covalent σ bonds in graphene.[26] The mechanical strength of a scaffold should be consistent with the target tissue. Scaffolds should be able to withstand the wear and tear at the site of implantation and also support the developing neotissue. However, according to Alsafadi and colleagues (2020), the tensile strength of the polymer is influenced by the 3-HV mol% which is in turn influenced by the carbon/nitrogen ratio and the type of nitrogen source used.[55] Inorder to facilitate angiogenesis and development of other structures like nerve bundles and lymphatic system, the composite should have similar mechanical properties as that of skin. For skin tissue engineering, the tensile strength varies between 5 to 30 MPa with young modulus and elongation at break above 4.6 MPa and 35% respectively.[56] The tensile strength of human skin lies in the range of 1–32 MPa. This variation is due to age, genetics, and skin color.[57] The tensile strength of haloarchaeal PHBV, its blend/composite lies within this range.

5.2.5 DSC-TGA. TG/DTG curves for haloarchaeal PHBV and its blend and composite are shown in Fig. 4b and ESI data S2.† All the films were stable up to 200 °C. The weight loss in the region from room temperature to 200 °C could be attributed to loss of moisture. The thermal degradation of PHBV showed a two step degradation in the regions 219–243 °C and 425–481 °C respectively. The weight loss is due to random chain scission. The depolymerisation may be induced by β-elimination and α-protonation. A slow degradation for PCL starts at 277 °C, continues to 360 °C and a major weight loss in the region 360 °C to 490 °C is observed due to complete breakdown of the polymer backbone due to pyrolysis. On the other hand a single step degradation was observed for PLLA in the temperature range 300–400 °C due to random scission of polymer chain. The PHBV/PLLA/PCL/GNP nanocomposite showed a three step degradation, Step-I of the three-step degradation of the nanocomposite occurred from 196.62 °C to 242.36 °C. Step-II from 277.24 °C to 298.08 °C and Step-III from 431.85 °C to 465.79 °C. Step I and Step III can be attributed to weight loss due to PHBV, whereas Step II may be due to the presence of GNPs.[58] A significant increase in char yield was observed on incorporation of GNP for PHBV/GNP composites.[59] Usually a high inorganic residue is often obtained in bacterial synthesis of PHAs due to presence of inorganic salts and other media components.

Table 2 Mechanical properties of *Halogeometricum borinquense* E3 derived PHBV and its blend/composite

Sample ID	Young's modulus (MPa)	Ultimate tensile strength (UTS) (MPa)	Elongation at break (%)
Halogeometricum borinquense E3 derived PHBV	148.25 ± 2.1	1.42 ± 0.3	1.03 ± 0.2
PHBV/PLLA/PCL	352.75 ± 30	5.1 ± 0.5	4.11 ± 2.2
PHBV/PLLA/PCL/GNP	396.25 ± 42	13.94 ± 1.2	0.88 ± 0.1

The DSC curves for PHBV and its blends are shown in ESI data S2.† PCL shows an endothermic peak corresponding to its melting point (T_m) at 68 °C. For PLLA glass transition temperature (T_g) is observed at 49 °C and T_m at 156 °C. The absence of cold crystallization peak shows the absence of less stable α' state in PLLA. The presence of an endothermic peak at 73 °C may be due to vaporization of solvent molecule which is supported by ~13% wt loss in TGA curve below 100 °C. The DSC scan of PHBV shows Tc at 64 °C and a premelting peak near 133 °C which is just before the T_m at 144 °C. For PHBV/PLLA/PCL blend a shift in baseline corresponding to its T_g is observed at 57 °C and a flow temperature at 157 °C. The absence of a sharp peak corresponding to the melting shows an increase in the amorphous nature of the blend. Similarly for PHBV/PLLA/PCL/GNP composites T_g is observed at a higher temperature *i.e.* at 59 °C as compared to PHBV which is usually between −5 to 5 °C. This shows the more ordered state of polymeric chains. The flow temperature is observed at 157 °C.

5.2.6 Swelling percentage and porosity. The swelling % of the polymer and its blend/composite is shown in Fig. 5a. The *Hgm. borinquense* E3 derived PHBV film demonstrated swelling of 173.79% after 1 hour. The PHBV/PLLA/PCL showed a reduction in the swelling percentage down to 98.24% while the PHBV/PLLA/PCL/GNP swelled to only 60.91% in 1 hour. The percentage porosity of the material was calculated by the solvent displacement method and was found to be 47.67%. The porosity % of the PHBV/PLLA/PCL was found to be 28.60%. The PHBV/PLLA/PCL/GNP composite showed a porosity percentage of 9.78%. After 24 hours, the pores were saturated with water and no more swelling occurred. The swelling percentage of haloarchaeal PHBV stabilized at 157.7%. The swelling percentages of PHBV/PLLA/PCL and PHBV/PLLA/PCL/GNP composites after 24 hours were observed to be 58.65% and 48.64% respectively. The assessment of the degree of swelling and water uptake of the biomaterial is important in determining its application. Swelling ability provides hydration, allows diffusion of serum proteins and growth factors, aids in controlled release of bioactive agents *etc.* Excessive swelling may be detrimental to the cells and could also compromise mechanical stability.[60] The higher swelling percentage of the haloarchaeal PHBV film can be attributed to its semi-crystalline nature where the amorphous regions interact more with the water molecules. The % porosity of the films is shown in Fig. 5b. The presence of numerous pores of random sizes formed due to the evaporation of chloroform after solvent casting, and the amount of the hydroxyvalerate (HV) units in the polymer chain also influence the swelling behavior. The pore size in the PHBV/PLLA/PCL blend was less than that of the *Hgm. borinquense* E3 derived native PHBV film and there was an increase in the crystalline behavior. This could be the reason for a reduced swelling ability. In the case of the PHBV/PLLA/PCL/GNP composite, the GNPs occupy the pores and the surface of the film further reducing the swelling. GNPs integrate within the polymer matrix forming a barrier, leading to improved mechanical strength and restricting the swelling.[61]

5.3 Biological characterisation

5.3.1 Assessment of *in vitro* biocompatibility. The PHBV/PLLA/PCL blend showed maximum viability of both the HaCaT cells as well as the L929 cells, right from day 1 throughout the experiment compared to the tissue culture grade control. This is a synergistic effect seen as neat PCL and PLLA did not yield good results.[62,63] The PHBV/PLLA/PCL/GNP nanocomposite was a close second followed by the haloarchaeal PHBV film. The cell viability showed a temporary decline on day 2. A possible explanation for this phenomenon could be the stress due to the introduction into a new growth environment. The cells overcome the initial stress and activate the mechanism for repair, growth, and metabolism thereby leading to an increase in the viability on day 5. The addition of GNP to the PHBV/PLLA/PCL blend reduces the cell viability albeit not significantly (Fig. 6a and b). The haloarchaeal PHBV film showed lower cell viability than the blend/composite. However, it was higher than the control. Human skin fibroblast (CCD-986Sk) cells grown on electrospun poly vinyl alcohol/glucose/reduced graphene oxide exhibited excellent growth of the fibroblasts and greatly increased the metabolic activity of the cells.[64] *In vitro* evaluation of human fibroblast cells on chitosan/polyvinylpyrrolidone/graphene oxide (GO) nanosheets showed improved cell viability in the presence of GO. *In vivo*

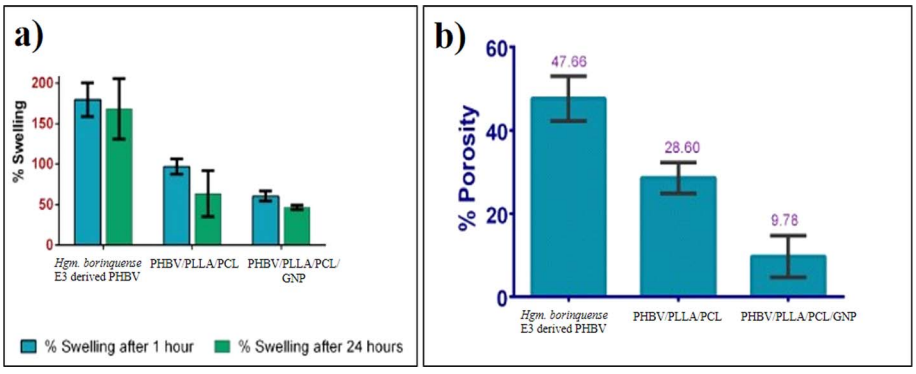

Fig. 5 (a) Percentage swelling ratio of PHBV film derived from *Halogeometricum borinquense* E3 and its blend/ composite after 1 hour and 24 hours. (b) Percentage porosity of PHBV film derived from *Halogeometricum borinquense* E3 and its composites by solvent displacement method.

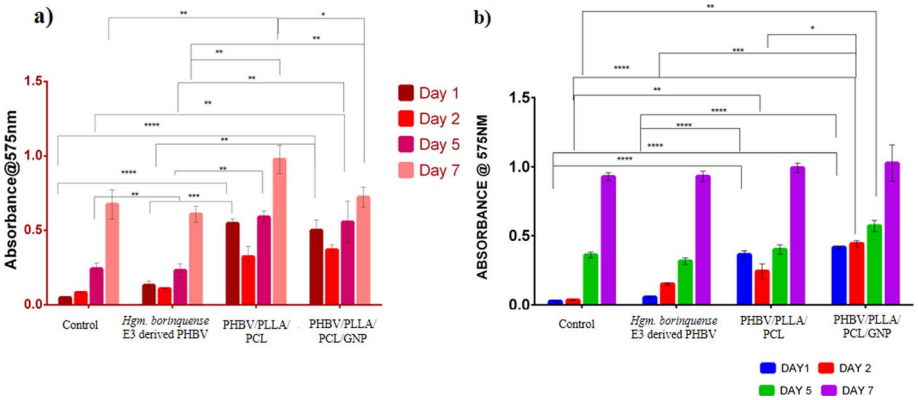

Fig. 6 Assessment of *in vitro* biocompatibility of the *Hgm. borinquense* E3 derived PHBV film and its blend/composite using (a) HaCaT cells and (b) L929 cells. Differences were analyzed with Two-way ANOVA with Tukey's multiple comparisons test. ****($p \leq 0.0001$), ***($p \leq 0.001$), **($p \leq 0.01$), *($p \leq 0.05$). $p > 0.05$ was considered non-significant.

studies using the same nanosheet confirmed faster wound healing with the incorporation of GO.[65] Human dermal fibroblast cells showed accelerated attachment and proliferation when grown on GO decorated poly(lactic-*co*-glycolic acid)/collagen scaffold than on the scaffold without GO.

5.3.2 Microscopy. The confocal (Fig. 7a and b) and the SEM (Fig. 8a and b) images demonstrate the attachment of HaCaT and L929 not only on the surface of the films but also inside the pores. The large HaCaT cells are observed to be growing in the form of clusters while the fibroblast cells are seen extending their filopodia to interact with the adjacent cells. *In vitro* studies reported by Kalva *et al.* 2023 (ref. 66) using 3T3 fibroblast cells showed that addition of PHBV to PCL in an air-spun scaffold improved initial cell attachment and faster cell proliferation than in the PCL scaffold alone. *In vivo* studies on rat model showed incorporation of the scaffold in the tissue without adverse inflammatory reaction.

5.3.3 Adsorption of proteins on the surface of the films. The haloarchaeal PHBV showed the maximum adsorption of proteins with an average of 9.88 μg of proteins adsorbed per mm^3 of the scaffold. This was followed by the PHBV/PLLA/PCL/GNP composite which adsorbed 7.46 μg mm^{-3}. The PHBV/PLLA/PCL adsorbed 6.56 μg mm^{-3} of protein (Fig. 9a). The surface adsorption of proteins is influenced by the physicochemical properties of the biomaterial, protein affinity, and diffusion. There is an immediate interaction of the biomaterial with proteins forming a dynamic monolayer on the surface. This is followed by the interaction between the cells and the biomaterial. The haloarchaeal PHBV was observed to adsorb maximum proteins. This could be due to the chemical composition of the native polymer and the nature of the surface topography facilitating a stronger interaction and adsorption of proteins. PHBV/PLLA/PCL/GNP composite was expected to show higher adsorption of proteins owing to its larger surface area. However, the slight reduction in the adsorption of proteins could be due to the presence of some hindering components.[67] The binding of the proteins reveal the biocompatible characteristics of the films for tissue engineering.

5.3.4 Degradation of the films *in vitro*. The native PHBV polymer derived from *Halogeometricum borinquense* E3 showed maximum degradation followed by the PHBV/PLLA/PCL blend and lastly the PHBV/PLAA/PCL/GNP nanocomposite (Fig. 9b). The haloarchaeal PHBV polymer fragmented into smaller pieces indicating its weak structural integrity. This is confirmed by the ultrastructure of the polymer which shows wider pores and deep cracks on the polymer (ESI data S3†). At the end of 28 days, the PHBV polymer showed an average 62.07% of degradation. The rate of degradation in the blend was slow with an average 13.07% in PHBV/PLLA/PCL and 8.62% degradation in PHBV/PLLA/PCL/GNP respectively. In the inflammatory stage of wound healing, polymorphonuclear leucocytes are responsible for the secretion of lysozyme which acts on the macromolecules degrading them to smaller units. The native PHBV film showed a higher weight loss than the blend or composite. The low tensile strength of the polymer caused it to fragment into smaller pieces. This could have exposed the sites for lysozyme action ultimately leading to weight loss.[68] The rate of degradation of the scaffolds should go hand-in-hand with the rate of the formation of the neo-tissue and allow the cells to secrete the extracellular matrix.

5.3.5 Evaluation of hemocompatibility of the films. Excellent hemocompatibility of haloarchaeal PHBV, its blends and composite was seen. The PHBV derived from *Hgm. borinquense* E3 resulted in a percentage hemolysis of 0.039%. The PHBV/PLLA/PCL blend demonstrated 0.352% hemolysis while the PHBV/PLLA/PCL/GNP composite caused 1.095% hemolysis. Scaffolds that cause hemolysis of less than 5% are classified as highly hemocompatible; between 5–10% as hemocompatible and greater than that as non-hemocompatible[69] (Table 3). The graphene nanocomposite provoked a higher hemolysis albeit less than 5%. The erythrocytes could have encountered the sharper edges of the GNPs ergo causing the damage.[70] The greater the degree of hemolysis, the lower the compatibility.[71,72] Lysis of the membrane of the erythrocytes releases hemoglobin in the supernatant which is correlated with the rate of hemolysis.[73] The haloarchaeal PHBV derived blends and composite

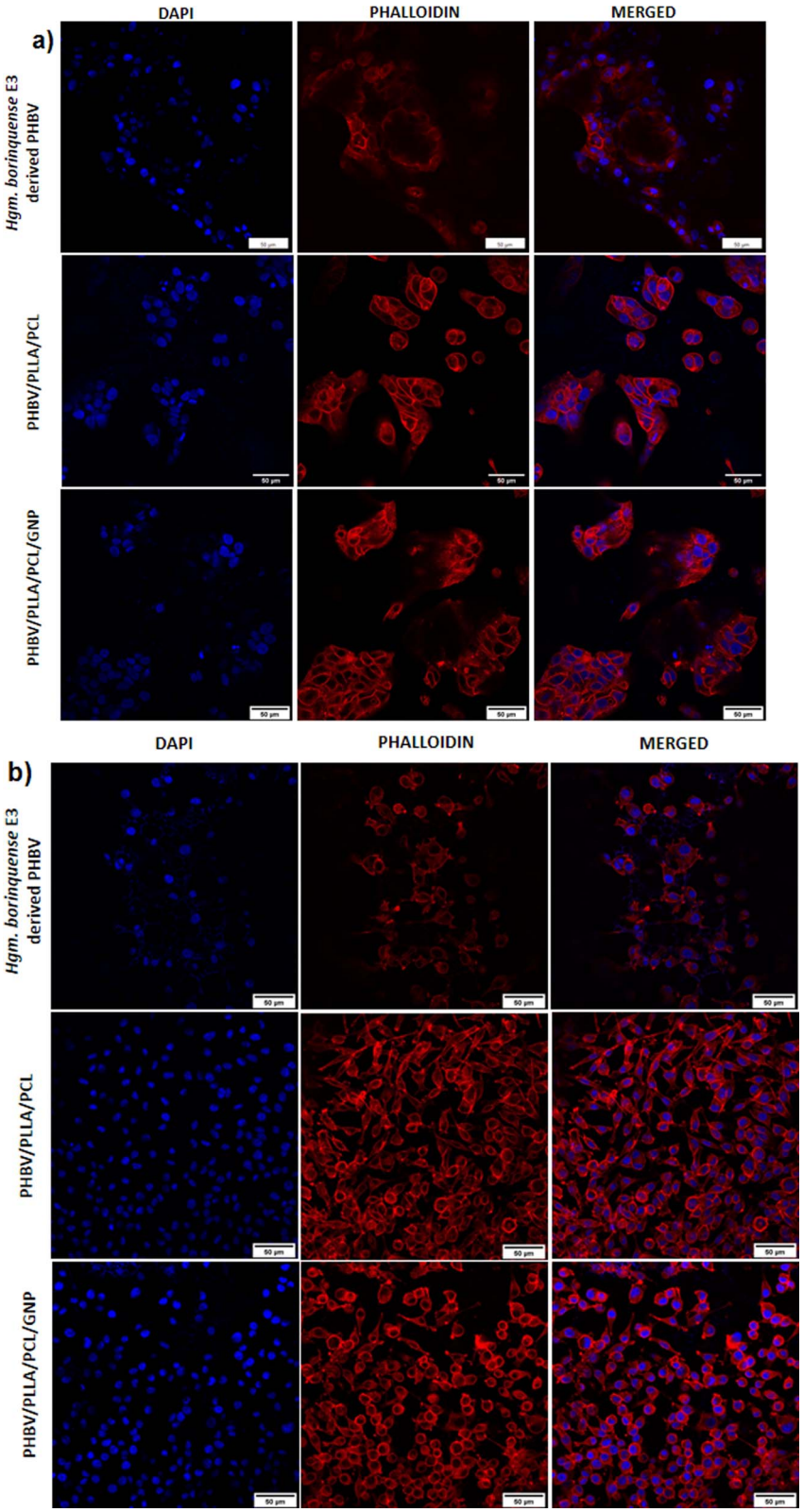

Fig. 7 (a) HaCaT cells and (b) L929 cells cultured on *Halogeomtericum borinquense* E3 derived PHBV, PHBV/PLLA/PCL and PHBV/PLLA/PCL/GNP films, stained with phalloidin and counterstained with DAPI visualized under confocal microscope (magnification 40×; scale bar: 50 μm).

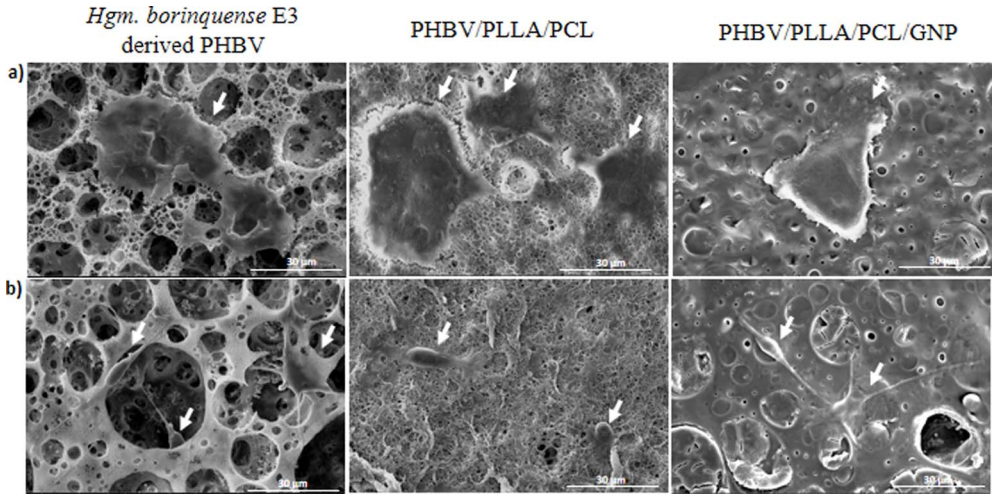

Fig. 8 FESEM images of (a) HaCaT cells and (b) L929 cells cultured on *Halogeomtericum borinquense* E3 derived PHBV, PHBV/PLLA/PCL and PHBV/PLLA/PCL/GNP films (magnification 4000×; scale bar 30 μm).

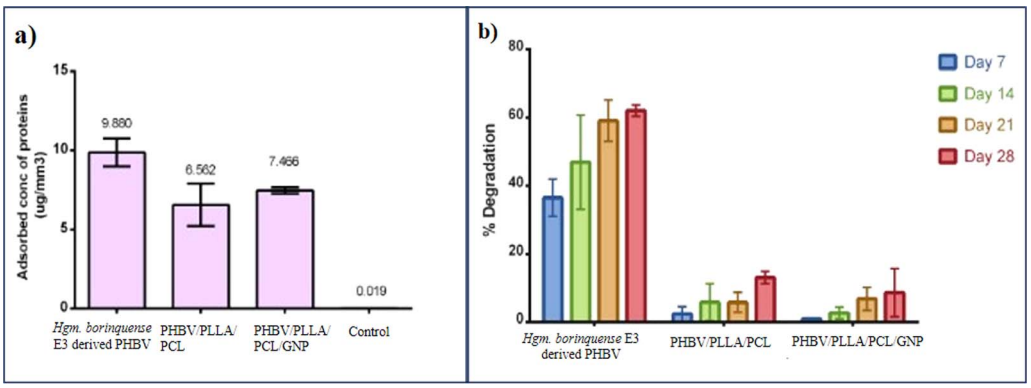

Fig. 9 (a) Protein adsorption study on the surface of the haloarchaeal PHBV film and its blend/composites. The concentration of protein adsorbed on the surface is represented as μg mm^{-3}. (b) A profile of *in vitro* degradation of the haloarchaeal PHBV and its blend/composites for 28 days.

Table 3 Hemocompatibility of *Halogeometricum borinquense* E3 derived PHBV and its blends/composite

Sample	Absorbance	% hemolysis	Remarks
Hgm. borinquense E3 derived PHBV	0.01	0.0391	Highly hemocompatible
PHBV/PLLA/PCL	0.018	0.3522	Highly hemocompatible
PHBV/PLLA/PCL/GNP	0.037	1.0958	Highly hemocompatible
Positive control	2.564	NA	
Negative control	0.009	NA	

showed less than 5% hemolysis and are therefore highly hemocompatible materials.

6 Conclusion

The current study focussed on the development of a blend/nanocomposite using an innately synthesized copolymer PHBV by *Halogeometricum borinquense* E3. The mechanical strength of the haloarchaeal PHBV was successfully improved by blending with PLLA, PCL and/or reinforcing it with 0.3% w/v of GNP. A comparative study of its physicochemical and biological properties was carried out. The haloarchaeal PHBV had a higher porosity (47.67%) and demonstrated greater swelling than the PHBV/PLLA/PCL blend, followed by the PHBV/GNP composite. *Halogeometricum borinquense* E3 derived PHBV also adsorbed the maximum proteins per mm^3 of its surface area. The trend that was seen in the case of protein adsorption is native PHBV > PHBV/PLLA/PCL/GNP composite > PHBV/PLLA/PCL. The cell viability of the PHBV/PLLA/PCL was significantly higher than the tissue culture grade control and even native PHBV. The

incorporation of GNP into the composite did not cause any significant change in the viability of the cells or hemocompatibility. Therefore, this nanocomposite can be used as potential novel biomaterial in skin tissue regeneration.

Data availability

The data supporting this article have been included as part of the ESI.†

Conflicts of interest

There are no conflicts to declare.

Acknowledgements

Anasuya Ganguly and Judith M. Bragança are grateful to Department of Biotechnology, Ministry of Science and Technology, Government of India for funding under DBT Builder – BITS Pilani KK Birla Goa Campus Interdisciplinary Life Science Programme for Advance Research and Education (Level III) BT/INF/22/SP2543/2021. Judith M. Braganca also thanks DST&WM, Government of Goa for the Research Grant. The authors are grateful to the Central Sophisticated Instrumentation Facility (CSIF), BITS Pilani Goa Campus. The authors would like to acknowledge Ms Mamta Mestry, Technical Assistant, Department of Chemical Engineering BITS Pilani KK Birla Goa Campus, for her help in DSC-TGA and FTIR analysis. The authors are grateful to Ms Navodipa Bhattacharya and Prof. Dibakar Chakrabarty for their help in bicinchoninic acid (BCA) assay. Prajakta Praveen Bhende thanks Birla Institute of Technology and Sciences, Pilani, KK Birla Goa Campus for the Institute Fellowship.

References

1 D. Kucera, I. Pernicová, A. Kovalcik, *et al.*, Characterization of the promising poly(3-hydroxybutyrate) producing halophilic bacterium Halomonas halophila, *Bioresour. Technol.*, 2018, **256**, 552–556, DOI: **10.1016/j.biortech.2018.02.062**.

2 M. R. Singh, S. Patel and D. Singh, *Natural Polymer-based Hydrogels as Scaffolds for Tissue Engineering*, Elsevier Inc., 2016, DOI: **10.1016/B978-0-323-42865-1.00009-X**.

3 H. M. Chang, Z. H. Wang, H. N. Luo, *et al.*, Poly(3-hydroxybutyrate-co-3-hydroxyhexanoate)- based scaffolds for tissue engineering, *Braz. J. Med. Biol. Res.*, 2014, **47**(7), 533–539, DOI: **10.1590/1414-431X20143930**.

4 P. X. Ma, Scaffolds for tissue fabrication, *Mater. Today*, 2004, **7**(5), 30–40, DOI: **10.1016/S1369-7021(04)00233-0**.

5 J. Możejko-Ciesielska and R. Kiewisz, Bacterial polyhydroxyalkanoates: Still fabulous?, *Microbiol. Res.*, 2016, **192**(2016), 271–282, DOI: **10.1016/j.micres.2016.07.010**.

6 S. Mohapatra, S. Maity, H. R. Dash, *et al.*, Bacillus and biopolymer: Prospects and challenges, *Biochem. Biophys. Rep.*, 2017, **12**, 206–213, DOI: **10.1016/j.bbrep.2017.10.001**.

7 M. E. Grigore, R. M. Grigorescu, L. Iancu, R. M. Ion, C. Zaharia and E. R. Andrei, Methods of synthesis, properties and biomedical applications of polyhydroxyalkanoates: a review, *J. Biomater. Sci., Polym. Ed.*, 2019, **30**(9), 695–712, DOI: **10.1080/09205063.2019.1605866**.

8 A. Anjum, M. Zuber, K. M. Zia, A. Noreen, M. N. Anjum and S. Tabasum, Microbial production of polyhydroxyalkanoates (PHAs) and its copolymers: A review of recent advancements, *Int. J. Biol. Macromol.*, 2016, **89**, 161–174, DOI: **10.1016/J.IJBIOMAC.2016.04.069**.

9 S. DasSarma, J. A. Coker and P. DasSarma, Archaea (overview), *Encyclopedia of Microbiology*, 3rd edn, 2009, pp. 1–23, DOI: **10.1016/B978-012373944-5.00108-5**.

10 B. Stres, M. J. Bonete, R. M. Martínez-Espinosa, I. Mahne and H. Bothe, Organisms of the Nitrogen Cycle Under Extreme Conditions: Low Temperature, Salinity, pH Value and Water Stress, *Biology of the Nitrogen Cycle*, 2007, 369–379, DOI: **10.1016/B978-044452857-5.50025-4**.

11 G. Y. A. Tan, C. L. Chen, L. Li, *et al.*, Start a Research on Biopolymer Polyhydroxyalkanoate (PHA): A Review, *Polymers*, 2014, **6**(3), 706–754, DOI: **10.3390/POLYM6030706**.

12 J. Ramier, T. Bouderlique, O. Stoilova, *et al.*, Biocomposite scaffolds based on electrospun poly(3-hydroxybutyrate) nanofibers and electrosprayed hydroxyapatite nanoparticles for bone tissue engineering applications, *Mater. Sci. Eng., C*, 2014, **38**(1), 161–169, DOI: **10.1016/j.msec.2014.01.046**.

13 J. Sun, J. Wu, H. Li and J. Chang, Macroporous poly(3-hydroxybutyrate-co-3-hydroxyvalerate) matrices for cartilage tissue engineering, *Eur. Polym. J.*, 2005, **41**(10), 2443–2449, DOI: **10.1016/J.EURPOLYMJ.2005.04.039**.

14 N. Pramanik, T. Mitra, M. Khamrai, *et al.*, Characterization and evaluation of curcumin loaded guar gum/polyhydroxyalkanoates blend films for wound healing applications, *RSC Adv.*, 2015, **5**(78), 63489–63501, DOI: **10.1039/C5RA10114J**.

15 S. J. Armstrong, M. Wiberg, G. Terenghi and P. J. Kingham, ECM Molecules Mediate Both Schwann Cell Proliferation and Activation to Enhance Neurite Outgrowth, *Tissue Eng., Part A*, 2007, **13**(12), 2863–2870, DOI: **10.1089/TEN.2007.0055**.

16 F. Opitz, K. Schenke-Layland, W. Richter, *et al.*, Tissue engineering of ovine aortic blood vessel substitutes using applied shear stress and enzymatically derived vascular smooth muscle cells, *Ann. Biomed. Eng.*, 2004, **32**(2), 212–222, DOI: **10.1023/B:ABME.0000012741.85600.F1/METRICS**.

17 G. Q. Chen and Q. Wu, The application of polyhydroxyalkanoates as tissue engineering materials, *Biomaterials*, 2005, **26**(33), 6565–6578, DOI: **10.1016/J.BIOMATERIALS.2005.04.036**.

18 Y. He, Z. Hu, M. Ren, *et al.*, Evaluation of PHBHHx and PHBV/PLA fibers used as medical sutures, *J. Mater. Sci.: Mater. Med.*, 2014, **25**(2), 561–571, DOI: **10.1007/S10856-013-5073-4/METRICS**.

19 Ł. Kaniuk and U. Stachewicz, Development and Advantages of Biodegradable PHA Polymers Based on Electrospun

PHBV Fibers for Tissue Engineering and Other Biomedical Applications, *ACS Biomater. Sci. Eng.*, 2021, **7**(12), 5339–5362, DOI: 10.1021/ACSBIOMATERIALS.1C00757.

20 J. Wu, J. Sun and J. Liu, Evaluation of PHBV/calcium silicate composite scaffolds for cartilage tissue engineering, *Appl. Surf. Sci.*, 2014, **317**, 278–283, DOI: 10.1016/j.apsusc.2014.08.101.

21 A. D. Dalgic, D. Atila, A. Karatas, A. Tezcaner and D. Keskin, Diatom shell incorporated PHBV/PCL-pullulan co-electrospun scaffold for bone tissue engineering, *Mater. Sci. Eng., C*, 2019, **100**, 735–746, DOI: 10.1016/j.msec.2019.03.046.

22 R. Naseem, L. Zhao, Y. Liu and V. V. Silberschmidt, Experimental and computational studies of poly-L-lactic acid for cardiovascular applications: recent progress, *Mech. Adv. Mater. Mod. Process.*, 2017, **3**(1), 1–18, DOI: 10.1186/S40759-017-0028-Y.

23 E. Capuana, F. Lopresti, M. Ceraulo and V. La Carrubba, Poly-l-Lactic Acid (PLLA)-Based Biomaterials for Regenerative Medicine: A Review on Processing and Applications, *Polym*, 2022, **14**, 1153, DOI: 10.3390/POLYM14061153.

24 M. Jamal, F. Sharif, M. M. Shozab, *et al.*, Development of Biocompatible Electrospun PHBV-PLLA Polymeric Bilayer Composite Membranes for Skin Tissue Engineering Applications, *Molecules*, 2024, **29**(9), 2049, DOI: 10.3390/molecules29092049.

25 P. Goodarzi, K. Falahzadeh, M. Nematizadeh, *et al.*, Tissue engineered skin substitutes, *Adv. Exp. Med. Biol.*, 2018, **1107**, 143–188, DOI: 10.1007/5584_2018_226/COVER.

26 S. R. Shin, Y. C. Li, H. L. Jang, *et al.*, Graphene-based materials for tissue engineering, *Adv. Drug Delivery Rev.*, 2016, **105**, 255–274, DOI: 10.1016/J.ADDR.2016.03.007.

27 S. Darvishi, S. Ahadian, H. Savoji and H. Savoji, Graphene-Based Nanomaterials in Tissue Engineering and Regenerative Medicine, *Handb Graphene*, 2019, vol. 2, pp. 637–658, DOI: 10.1002/9781119468455.ch38.

28 Y. Chang, S. T. Yang, J. H. Liu, *et al.*, In vitro toxicity evaluation of graphene oxide on A549 cells, *Toxicol. Lett.*, 2011, **200**(3), 201–210, DOI: 10.1016/j.toxlet.2010.11.016.

29 B. Salesa, A. Tuñón-Molina, A. Cano-Vicent, M. Assis, J. Andrés and Á. Serrano-Aroca, Graphene Nanoplatelets: In Vivo and In Vitro Toxicity, Cell Proliferative Activity, and Cell Gene Expression, *Appl. Sci.*, 2022, **12**(2), 720, DOI: 10.3390/app12020720.

30 P. Suvarnaphaet, S. Sasivimolkul, C. Sukkasem, *et al.*, Biodegradable Electrode patch made of Graphene/PHA for ECG detecting Applications, in *2019 12th Biomedical Engineering International Conference (BMEiCON)*, IEEE, 2019, pp. 1–5, DOI: 10.1109/BMEiCON47515.2019.8990243.

31 M. Moschetta, M. Chiacchiaretta, F. Cesca, *et al.*, Graphene Nanoplatelets Render Poly(3-Hydroxybutyrate) a Suitable Scaffold to Promote Neuronal Network Development, *Front. Neurosci.*, 2021, **15**, 1–12, DOI: 10.3389/fnins.2021.731198.

32 B. B. Salgaonkar and J. M. Bragança, Biosynthesis of poly(3-hydroxybutyrate-co-3-hydroxyvalerate) by Halogeometricum borinquense strain E3, *Int. J. Biol. Macromol.*, 2015, **78**, 339–346, DOI: 10.1016/j.ijbiomac.2015.04.016.

33 A. I. Aghmiuni, S. Heidari Keshel, F. Sefat and A. Akbarzadeh Khiyavi, Quince seed mucilage-based scaffold as a smart biological substrate to mimic mechanobiological behavior of skin and promote fibroblasts proliferation and h-ASCs differentiation into keratinocytes, *Int. J. Biol. Macromol.*, 2020, **142**, 668–679, DOI: 10.1016/J.IJBIOMAC.2019.10.008.

34 E. I. Shishatskaya, E. D. Nikolaeva, O. N. Vinogradova and T. G. Volova, Experimental wound dressings of degradable PHA for skin defect repair, *J. Mater. Sci.: Mater. Med.*, 2016, **27**(11), 1, DOI: 10.1007/s10856-016-5776-4.

35 P. Sangsanoh, N. Israsena, O. Suwantong and P. Supaphol, Effect of the surface topography and chemistry of poly(3-hydroxybutyrate) substrates on cellular behavior of the murine neuroblastoma Neuro2a cell line, *Polym. Bull.*, 2017, **74**(10), 4101–4118, DOI: 10.1007/s00289-017-1947-9.

36 A. Suslu, A. Z. Albayrak, E. Bayir, A. Sendemir Urkmez and U. Cocen, In Vitro Biocompatibility and Antibacterial Activity of Electrospun Ag Doped HAp/PHBV Composite Nanofibers, *Int. J. Polym. Mater. Polym. Biomater.*, 2015, **64**(9), 465–473, DOI: 10.1080/00914037.2014.977892.

37 A. L. Rivera-Briso, F. L. Aachmann, V. Moreno-Manzano and Á. Serrano-Aroca, Graphene oxide nanosheets versus carbon nanofibers: Enhancement of physical and biological properties of poly(3-hydroxybutyrate-co-3-hydroxyvalerate) films for biomedical applications, *Int. J. Biol. Macromol.*, 2020, **143**, 1000–1008, DOI: 10.1016/J.IJBIOMAC.2019.10.034.

38 K. T. Shalumon, K. H. Anulekha, K. P. Chennazhi, H. Tamura, S. V. Nair and R. Jayakumar, Fabrication of chitosan/poly(caprolactone) nanofibrous scaffold for bone and skin tissue engineering, *Int. J. Biol. Macromol.*, 2011, **48**(4), 571–576, DOI: 10.1016/j.ijbiomac.2011.01.020.

39 M. F. Abazari, Z. S. Karizi, N. Hajati-Birgani, M. Kohandani, S. Torabinejad, F. Nejati, N. Nasiri, M. H. Maleki, H. Mohajerani and V. Mansouri, Curcumin-loaded PHB/PLLA nanofibrous scaffold supports osteogenesis in adipose-derived stem cells in vitro, *Polym. Adv. Technol.*, 2021, **32**(9), 3563–3571, DOI: 10.1002/pat.5366.

40 F. Schlottmann, V. Bucan, P. M. Vogt and N. Krezdorn, A Short History of Skin Grafting in Burns: From the Gold Standard of Autologous Skin Grafting to the Possibilities of Allogeneic Skin Grafting with Immunomodulatory Approaches, *Medicina*, 2021, **57**(3), 225, DOI: 10.3390/medicina57030225.

41 S. Malfatti, B. J. Tindall, S. Schneider, *et al.*, Complete genome sequence of Halogeometricum borinquense type strain (PR3T), *Stand. Genomic Sci.*, 2009, **1**(2), 150, DOI: 10.4056/SIGS.23264.

42 R. Mahansaria, S. Bhowmik, A. Dhara, *et al.*, Production enhancement of poly(3-hydroxybutyrate-co-3-hydroxyvalerate) in Halogeometricum borinquense, characterization of the bioplastic and desalination of the bioreactor effluent, *Process Biochem.*, 2020, **94**, 243–257, DOI: 10.1016/J.PROCBIO.2020.04.004.

43 B. Salgaonkar and J. Bragança, Utilization of Sugarcane Bagasse by Halogeometricum borinquense Strain E3 for Biosynthesis of Poly(3-hydroxybutyrate-co-3-hydroxyvalerate), *Bioengineering*, 2017, **4**(2), 50, DOI: 10.3390/bioengineering4020050.

44 L. Suamte, A. Tirkey, J. Barman and P. Jayasekhar Babu, Various manufacturing methods and ideal properties of scaffolds for tissue engineering applications, *Smart Mater. Manuf.*, 2023, **1**, 100011, DOI: 10.1016/j.smmf.2022.100011.

45 R. Naseem, G. Montalbano, M. J. German, A. M. Ferreira, P. Gentile and K. Dalgarno, Influence of PCL and PHBV on PLLA Thermal and Mechanical Properties in Binary and Ternary Polymer Blends, *Molecules*, 2022, **27**, 7633, DOI: 10.3390/MOLECULES27217633.

46 G. Lutzweiler, A. Ndreu Halili and N. Engin Vrana, The Overview of Porous, Bioactive Scaffolds as Instructive Biomaterials for Tissue Regeneration and Their Clinical Translation, *Pharmaceutics*, 2020, **12**(7), 602, DOI: 10.3390/pharmaceutics12070602.

47 Z. Zhang, Y. Feng, L. Wang, D. Liu, C. Qin and Y. Shi, A review of preparation methods of porous skin tissue engineering scaffolds, *Mater. Today Commun.*, 2022, **32**, 104109, DOI: 10.1016/j.mtcomm.2022.104109.

48 Y. Zhou, M. Zhao, H. Guo, Y. Li, Q. Liu and B. Deng, Morphology and crystallization behavior of poly(3-hydroxybutyrate- co -3-hydroxyvalerate)/polyhedral oligomeric silsesquioxane hybrids, *RSC Adv.*, 2019, **9**(15), 8146–8158, DOI: 10.1039/C8RA09281H.

49 R. Balu, T. S. S. Kumar, M. Ramalingam and S. Ramakrishna, Electrospun Polycaprolactone/Poly(1,4-butylene adipate-co-polycaprolactam) Blends: Potential Biodegradable Scaffold for Bone Tissue Regeneration, *J. Biomater. Tissue Eng.*, 2011, **1**(1), 30–39, DOI: 10.1166/jbt.2011.1004.

50 J. Wang, L. Zhan, X. Zhang, R. Wu, L. Liao and J. Wei, Silver Nanoparticles Coated Poly(L-Lactide) Electrospun Membrane for Implant Associated Infections Prevention, *Front. Pharmacol*, 2020, **11**, 431, DOI: 10.3389/fphar.2020.00431.

51 R. Naseem, G. Montalbano, M. J. German, A. M. Ferreira, P. Gentile and K. Dalgarno, Influence of PCL and PHBV on PLLA Thermal and Mechanical Properties in Binary and Ternary Polymer Blends, *Molecules*, 2022, **27**(21), 7633, DOI: 10.3390/molecules27217633.

52 J. Ahmed, M. Z. Mulla, A. Vahora, A. Bher and R. Auras, Polylactide/graphene nanoplatelets composite films: Impact of high-pressure on topography, barrier, thermal, and mechanical properties, *Polym. Compos.*, 2021, **42**(6), 2898–2909, DOI: 10.1002/PC.26023.

53 S. Khasim, Polyaniline-Graphene nanoplatelet composite films with improved conductivity for high performance X-band microwave shielding applications, *Results Phys.*, 2019, **12**, 1073–1081, DOI: 10.1016/J.RINP.2018.12.087.

54 P. Kuppan, K. S. Vasanthan, D. Sundaramurthi, U. M. Krishnan and S. Sethuraman, Development of poly(3-hydroxybutyrate-co-3-hydroxyvalerate) fibers for skin tissue engineering: Effects of topography, mechanical, and chemical stimuli, *Biomacromolecules*, 2011, **12**(9), 3156–3165, DOI: 10.1021/bm200618w.

55 D. Alsafadi, O. Al-Mashaqbeh, A. Mansour and M. Alsaad, Optimization of nitrogen source supply for enhanced biosynthesis and quality of poly(3-hydroxybutyrate-co-3-hydroxyvalerate) by extremely halophilic archaeon Haloferax mediterranei, *Microbiologyopen*, 2020, **9**(8), e1055, DOI: 10.1002/MBO3.1055.

56 J. J. Elsner and M. Zilberman, Novel antibiotic-eluting wound dressings: An in vitro study and engineering aspects in the dressing's design, *J. Tissue Viability*, 2010, **19**(2), 54–66, DOI: 10.1016/j.jtv.2009.11.001.

57 W. J. Chong, S. Shen, Y. Li, *et al.*, Biodegradable PLA-ZnO nanocomposite biomaterials with antibacterial properties, tissue engineering viability, and enhanced biocompatibility, *Smart Mater. Manuf.*, 2023, **1**, 100004, DOI: 10.1016/J.SMMF.2022.100004.

58 B. Mensah, D. S. Konadu, F. Nsaful, P. N. Angnunavuri and S. Kwofie, A systematic study of the effect of graphene oxide and reduced graphene oxide on the thermal degradation behavior of acrylonitrile-butadiene rubber in air and nitrogen media, *Sci. Afr.*, 2023, **19**, e01501, DOI: 10.1016/j.sciaf.2022.e01501.

59 B. Sitharaman, S. Kanakia, J. Toussaint, *et al.*, Physicochemical characterization of a novel graphene-based magnetic resonance imaging contrast agent, *Int. J. Nanomed.*, 2013, 2821, DOI: 10.2147/IJN.S47062.

60 J. Li and D. J. Mooney, Designing hydrogels for controlled drug delivery, *Nat. Rev. Mater.*, 2016, **1**(12), 1–17, DOI: 10.1038/NATREVMATS.2016.71.

61 B. Yang, B. Nagarajan and P. Mertiny, Characterization of swelling behavior of carbon nano-filler modified polydimethylsiloxane composites, *J. Elastomers Plast.*, 2021, **53**(8), 955, DOI: 10.1177/00952443211006156.

62 A. O. Basar, S. Castro, S. Torres-Giner, J. M. Lagaron and H. Turkoglu Sasmazel, Novel poly(ε-caprolactone)/gelatin wound dressings prepared by emulsion electrospinning with controlled release capacity of Ketoprofen anti-inflammatory drug, *Mater. Sci. Eng., C*, 2017, **81**, 459–468, DOI: 10.1016/J.MSEC.2017.08.025.

63 P. P. Bhende, R. Chauhan, S. Waigaonkar, J. M. Bragança and A. Ganguly, Composites of Bacillus megaterium H16 derived poly-3-hydroxybutyrate as a biomaterial for skin tissue engineering, *Int. J. Biol. Macromol.*, 2023, **244**, 125355, DOI: 10.1016/j.ijbiomac.2023.125355.

64 K. B. Narayanan, G. T. Park and S. S. Han, Electrospun poly(vinyl alcohol)/reduced graphene oxide nanofibrous scaffolds for skin tissue engineering, *Colloids Surf., B*, 2020, **191**, 110994, DOI: 10.1016/j.colsurfb.2020.110994.

65 N. Mahmoudi, N. Eslahi, A. Mehdipour, *et al.*, Temporary skin grafts based on hybrid graphene oxide-natural biopolymer nanofibers as effective wound healing substitutes: pre-clinical and pathological studies in animal models, *J. Mater. Sci.: Mater. Med.*, 2017, **28**(5), 73, DOI: 10.1007/s10856-017-5874-y.

66 S. N. Kalva, Y. B. Dalvi, N. K. P, *et al.*, Air-jet spun PHBV/PCL blend tissue engineering scaffolds exhibit improved

mechanical properties and cell proliferation, *Results Mater.*, 2023, **19**, 100415, DOI: 10.1016/j.rinma.2023.100415.

67 S. G. Hu, C. H. Jou and M. C. Yang, Protein adsorption, fibroblast activity and antibacterial properties of poly(3-hydroxybutyric acid-co-3-hydroxyvaleric acid) grafted with chitosan and chitooligosaccharide after immobilized with hyaluronic acid, *Biomaterials*, 2003, **24**(16), 2685–2693, DOI: 10.1016/S0142-9612(03)00079-6.

68 A. Zonari, M. T. Cerqueira, S. Novikoff, *et al.*, Poly(hydroxybutyrate-co-hydroxyvalerate) Bilayer Skin Tissue Engineering Constructs with Improved Epidermal Rearrangement, *Macromol. Biosci.*, 2014, **14**(7), 977–990, DOI: 10.1002/MABI.201400005.

69 N. Kumar, D. Desagani, G. Chandran, *et al.*, Biocompatible agarose-chitosan coated silver nanoparticle composite for soft tissue engineering applications, *Artif. Cells, Nanomed., Biotechnol.*, 2018, **46**(3), 637–649, DOI: 10.1080/21691401.2017.1337021.

70 A. M. Pinto, J. A. Moreira, F. D. Magalhães and I. C. Gonçalves, Polymer surface adsorption as a strategy to improve the biocompatibility of graphene nanoplatelets, *Colloids Surf., B*, 2016, **146**, 818–824, DOI: 10.1016/J.COLSURFB.2016.07.031.

71 P. C. Caracciolo, M. I. Rial-Hermida, F. Montini-Ballarin, G. A. Abraham, A. Concheiro and C. Alvarez-Lorenzo, Surface-modified bioresorbable electrospun scaffolds for improving hemocompatibility of vascular grafts, *Mater. Sci. Eng., C*, 2017, **75**, 1115–1127, DOI: 10.1016/J.MSEC.2017.02.151.

72 A. A. Shitole, P. S. Giram, P. W. Raut, P. P. Rade, A. P. Khandwekar, N. Sharma and B. Garnaik, Clopidogrel eluting electrospun polyurethane/polyethylene glycol thromboresistant, hemocompatible nanofibrous scaffolds, *J. Biomater. Appl.*, 2019, **33**(10), 1327–1347, DOI: 10.1177/0885328219832984.

73 J. Horakova, P. Mikes, A. Saman, *et al.*, Comprehensive assessment of electrospun scaffolds hemocompatibility, *Mater. Sci. Eng., C*, 2018, **82**, 330–335, DOI: 10.1016/J.MSEC.2017.05.011.